Fourier Transform Infrared Spectroscopy: Fundamentals and Application in Functional Groups and Nanomaterials Characterization

Chapter · September 2018

DOI: 10.1007/978-3-319-92955-2_9

CITATIONS
83

READS
44,465

6 authors, including:

Shahid Ali Khan
National University of Sciences and Technology
98 PUBLICATIONS **2,305** CITATIONS

SEE PROFILE

Latif Ullah Khan
Synchrotron-Light for Experimental Science and Applications in the Middle East (…
49 PUBLICATIONS **574** CITATIONS

SEE PROFILE

Abdullah M. Asiri
King Abdulaziz University
3,124 PUBLICATIONS **101,321** CITATIONS

SEE PROFILE

Chapter 9
Fourier Transform Infrared Spectroscopy: Fundamentals and Application in Functional Groups and Nanomaterials Characterization

Shahid Ali Khan, Sher Bahadar Khan, Latif Ullah Khan, Aliya Farooq, Kalsoom Akhtar, and Abdullah M. Asiri

9.1 Introduction

Fourier transform infrared spectroscopy (FTIR) is a largely used technique to identify the functional groups in the materials (gas, liquid, and solid) by using the beam of infrared radiations. An infrared spectroscopy measured the absorption of IR radiation made by each bond in the molecule and as a result gives spectrum which is commonly designated as % transmittance versus wavenumber (cm^{-1}). A diverse range of materials containing the covalent bond absorbed electromagnetic radiation

S. A. Khan (✉)
Department of Chemistry, University of Swabi, Anbar-23561, Khyber Pakhtunkhwa, Pakistan

Center of Excellence for Advanced Materials Research, King Abdulaziz University, Jeddah, Saudi Arabia

Chemistry Department, Faculty of Science, King Abdulaziz University, Jeddah, Saudi Arabia
e-mail: skhan0034@stu.kau.edu.sa

S. B. Khan (✉) · A. M. Asiri
Center of Excellence for Advanced Materials Research, King Abdulaziz University, Jeddah, Saudi Arabia

Chemistry Department, Faculty of Science, King Abdulaziz University, Jeddah, Saudi Arabia
e-mail: sbkhan@kau.edu.sa

L. U. Khan
Brazilian Nanotechnology National Laboratory (LNNano), Brazilian Center for Research in Energy and Materials (CNPEM), Campinas, São Paulo, Brazil

A. Farooq
Department of Chemistry, Shaheed Benazir Bhutto Women University, Peshawar, Pakistan

K. Akhtar
Division of Nano Sciences and Department of Chemistry, Ewha Womans University, Seoul, South Korea

S. K. Sharma (ed.), *Handbook of Materials Characterization*,
https://doi.org/10.1007/978-3-319-92955-2_9

in the IR region. The IR region is at lower energy and higher wavelength than the UV-visible light and has higher energy or shorter wavelength than the microwave radiations. For the determination of functional groups in a molecule, it must be IR active. An IR active molecule is the one which has dipole moment. When the IR radiation interacts with the covalent bond of the materials having an electric dipole, the molecule absorbed energy, and the bond starts back and forth oscillation. Therefore, the oscillation which caused the change in the net dipole moment of the molecule should absorbed IR radiations.

A single atom doesn't absorb IR radiation as it has no chemical bond. Symmetrical molecules also do not absorbed IR radiation, because of zero dipole moment. For instance, H_2 molecule has two H atoms; both canceled the effect of each other and giving zero dipole moment to H_2 molecule. Therefore, H_2 molecule is not an IR active molecule. On other hand, H-F (hydrogen fluoride) is an IR active molecule, because when IR radiation interacts with H-F molecule, the charge transferred toward the fluorine atom and as a result fluorine becomes partial negative and hydrogen becomes partial positive, giving net dipole moment to H-F molecule.

It should be noted here that a particular IR radiation (frequency) will be absorbed by a particular bond in the molecule, because every bond has their particular natural vibrational frequency. For instance, a molecule such as acetic acid (CH_3COOH) containing various bonds (C-C, C-H, C-O, O-H, and C=O), all these bonds are absorbed at specific wavelength and are not affected by other bond. We can say that two molecules with different structures don't have the same infrared spectrum, although some of the frequencies might be same.

9.1.1 Electromagnetic Spectrum

The interaction of matter with any part of the electromagnetic spectrum is called spectroscopy, which is an instrumentally assisted study between matter and electromagnetic radiation of any range. Electromagnetic spectrum is composed of various radiations containing different wavelengths, which is a type of radiant energy, ranging from gamma rays to X-rays via visible light to radio waves, each of which can be considered as a wave or particle traveling at the speed of light. Electromagnetic radiations have a broad range of spectrum starting from the highest energy cosmic rays via X-rays, UV, Vis, infrared, micro-, and radio waves (Table 9.1). They propagate in vacuum with the speed of light. The electromagnetic radiations are described by the parameters like frequency, wavelength, and energy. The relationship between the frequency, wavelength, and energy is given as:

$$\begin{aligned} E &\propto f \\ E &= hf \end{aligned} \tag{9.1}$$

where E is the energy, f is the frequency of the electromagnetic radiations, and h is the Planck's constant which is equal to 6.634×10^{-34} J. s. The frequency and energy have direct relation, while both have indirect relation with the wavelength.

Table 9.1 Electromagnetic spectrum and molecular effects

Radiation	Wavelength (cm)	Energy (Kcal/mol)	Molecular effects	Approximate range of wavelength
Gamma rays	10^{-9}	10^{6}	Ionization	Atomic nuclei
X-ray	10^{-7}	10^{4}	Ionization	Atoms
Vacuum UV	10^{-5}	10^{-9}	Ionization	Molecules
Near UV	10^{-4}	10^{2}	Electronic transition	Protozoans
Visible	10^{-3}	10	Electronic transition	Needle point
Infrared	10^{-1}	10^{-2}	Molecular vibration	Butterfly
Microwaves	10^{2}	10^{-4}	Rotational motion	Human
Radio wave	10^{4}	10^{-6}	Nuclear spin transition	Buildings

$$\begin{aligned} f &\infty \tfrac{1}{\lambda} \\ E &= \tfrac{hc}{\lambda} \end{aligned} \tag{9.2}$$

where c is the speed of light which is equal to 3×10^8 m/s and λ is the wavelength of light.

Chemists used selectively the electromagnetic radiations to explore the complete structural, chemical, and physical properties of the molecules.

9.1.2 Infrared

The IR region is lying between visible and microwave end of the electromagnetic radiation spectrum. It is basically divided into three main portions: near IR (14000–4000 cm^{-1}), mid-IR (4000–400 cm^{-1}), and far IR (400–40 cm^{-1}). IR spectroscopy is an advanced and extensively used analytical tool that investigates the structural chemistry of the sample by irradiating with IR radiations. The molecules or sample absorbed the IR radiations and displayed an absorption spectrum. IR measured the amount of radiations absorbed by the molecule and their intensity. The absorption of the IR radiations causes various molecular motions in the molecule, which create a net dipole moment. Therefore, a molecule is said to be IR active if the molecule has a net dipole moment (e.g., CH_4, C_2H_6, NO_2, TiO_2), otherwise it will be IR inactive (e.g., H_2, O_2, etc.). One of main advantages of FTIR spectroscopy is its capability to identify functional groups such as C=O, C-H, or N-H. FTIR spectroscopy enables by measuring all types of samples: solids, liquids, and gases.

9.1.3 Infrared Spectrum

The plot of measured infrared light intensity (absorbance or % transmittance) versus its property, such as energy range expressed in wavenumber (cm^{-1}), is called an infrared spectrum. The infrared spectrum is conventionally plotted with high wavenumber to the left and low wavenumber to the right in its x-axis. Plots of the typical FTIR spectra should always follow this convention. However, in certain articles the contrary profile of FTIR spectra are also reported (Fig. 9.1). The IR spectrum is recorded in absorbance mode, which measures the amount of light absorbed by a sample, and its intensity at y-axis is plotted in absorbance unit. As shown in Fig. 9.1, the absorption band of each characteristic functional group in compound is pointed up, and their tops represent wavenumbers at which significant amounts of IR light were absorbed by the sample. The absorbance spectrum of a sample is calculated from the following relation:

$$A = \log (I_0/I) \tag{9.3}$$

where A, absorbance: I_0, intensity in the background spectrum; and I, intensity in the spectrum of sample. The absorbance can be also correlated with the concentration of molecules in a sample through the equation called as Beer's law:

$$A = \varepsilon lc \tag{9.4}$$

where, A absorbance; ε, molar absorptivity; l, path length; and c, concentration of the sample. The height or area of a peak in an absorbance spectrum is proportional to concentration; therefore Beer's law can be used to determine the concentrations of molecules in samples.

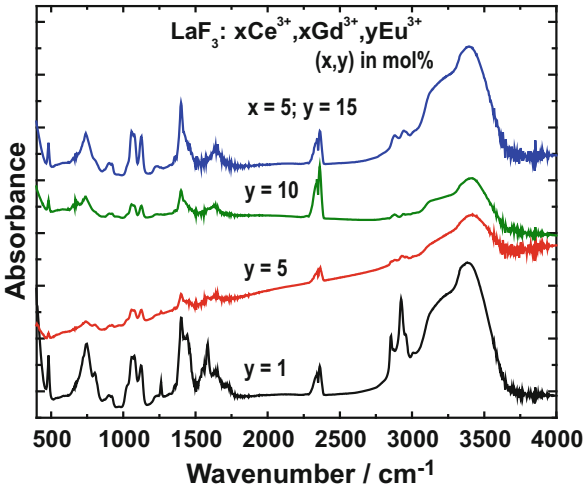

Fig. 9.1 FTIR spectra of LaF_3:$x$$Ce^{3+}$, $x$$Gd^{3+}$,$y$$Eu^{3+}$($x = 5$; $y = 1$, 5, 10 and 15 mol%) nanomaterials functionalized with oleic acid [1]

In the given example (Fig. 9.1), we have explained the FTIR spectra of oleic acid coated LaF_3:xCe^{3+}, xGd^{3+}, yEu^{3+} NPs [1] for the sake of understanding of the nonspecialized readers. The FTIR spectra of these nanomaterials are dominated by broad and intensive absorption band at 3400 cm^{-1} corresponding to the O-H stretching vibrations (asymmetric and symmetric) of the adsorbed water molecules with the existence of O-H deformation (σ) vibrational around 1640 cm^{-1}. The absorption bands around 2930 and 1390 cm^{-1} are attributed to the $\nu_{C\text{-}H}$ of CH_2 groups present in oleic acid, revealing the presence of organic surfactant on surface of LaF_3:*x*Ce^{3+}, *x*Gd^{3+}, *y*Eu^{3+} NPs. A closer look revealed the appearance of two absorption peaks around 1582 and 1546 cm^{-1}, which is attributed to the characteristic of the asymmetric (COO–) stretching and the symmetric (COO–) stretching. However, this analysis gives no information about the presence of LaF_3 phase, because $\nu_{Ln\text{-}F}$ is generally observed below 400 cm^{-1}.

On the other hand, the *y*-axis of an infrared spectrum can be also plotted in unit called percent transmittance (% T), which measures the percentage of light transmitted by the compound and can be calculated as follows:

$$\%T = 100 \times (I/I_0) \tag{9.5}$$

where % *T*, percent transmittance; I_0, intensity in the background spectrum; and *I*, intensity in the sample spectrum.

It is noteworthy that in the % *T* spectrum, the band of each characteristic functional group of the compound is pointed down, as shown in Fig. 9.2. Absorbance and % *T* are mathematically related to each other, and they are interconvertible using FTIR software. This conversion causes change of the *y*-axis, but the peak positions are not affected. In the scientific literature, the FTIR spectra are usually plotted in both absorbance and % *T* units.

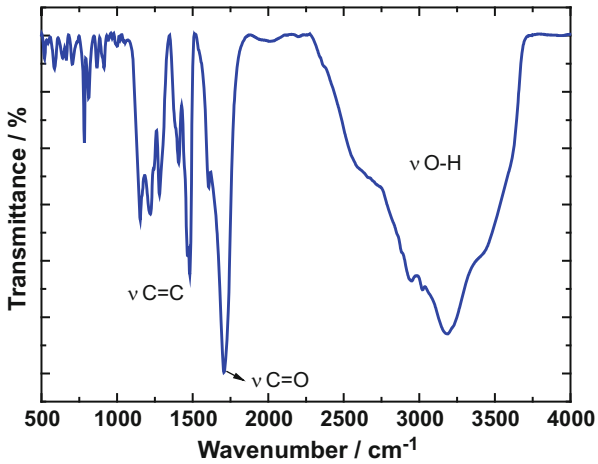

Fig. 9.2 FTIR absorption spectrum of p-tetrakis (carboxymethyl)calix-4-arene tetrol macrocycle ligand [2]

9.2 Brief History of FTIR

The development of spectroscopy in non-visual wavelengths (IR region) was advanced simultaneously with the development of visual spectroscopy. Infrared light was first discovered by Sir Frederick William Herschel during his experiment, which was performed with mercury-in-glass thermometers illuminated by sunlight dispersed through a glass prism (Herschel 1800). He was really surprised when he found that not only the thermometers register heat beyond the red end of the visible spectrum, but the greatest amount of heat was found in this region [3]. Later on, various scientists, including William Herschel's son, Sir John Frederick William Herschel, contribute to the infrared spectroscopy very effectively to measure the infrared spectrum practically. Jacquinot [4], Fellgett [5], and Connes [6] are the famous researchers along with other known scientists for their work in the early history of spectroscopy [7, 8]. The work of Rubens and Wood on FTIR interferogram [9] and Rubens and von Baeyer in spectroscopy [10] was known before the advent of Michelson interferometer [11]. However, before 1980 some domestic high-resolution FTIR spectrometers were also reported [12–14].

In the mid-1960s, progress has been made in the infrared microscopy and developed techniques which enhanced the signal-to-noise ratio. In the late 1970s, the infrared microscope systems were introduced in the market and in the early stages of 1980s by Digilab and Spectra-Tech Company.

However, the real advancement was made in FTIR spectroscopy with the availability of commercially accessible high-resolution instruments. Later on, the scientists focused their attention on innovation, queries, and evolutions of the essential theoretical and spectroscopic procedures. Erstwhile to 1980, the FTIR spectrometers resolution was 0.04 cm^{-1} which is inadequate and less efficient than the old-fashioned grating apparatuses. Revolution attained with the Bomem instruments having a maximum optical path difference ($^{d}_{\mathrm{MOPD}}$) = 250 cm^{-1}, associated to the unapodized resolution which is $\Delta\tilde{\nu} = 0.61^{d-1}_{\mathrm{MOPD}} = 0.0024\ cm^{-1}$.

In the traditional IR spectroscopy, specific IR radiations are selected for the analysis, which is a tedious and time-consuming process. For example, a molecule containing O-H and C=O functional groups, different ranges of IR radiation were applied for the determination of O-H and C=O functional groups. This problem was solved with the advent of Fourier transform infrared spectroscopy (FTIR), where a pulse (burst of energy) is bombarded on molecules; as a result, different parts of the same molecules received its characteristics IR radiation and displayed a time domain spectrum called interferogram. The time domain spectrum (interferogram) is converted to frequency domain spectrum by the application of mathematical procedure known as Fourier transform.

9.3 Matter-Energy Interaction

When electromagnetic radiation interacts with a material, for example, UV-Vis light, the excitation of electrons occurs from the highest occupied molecular orbital (HOMO) to lowest unoccupied molecular orbital (LUMO). This movement of an electron from a lower energy level to a higher energy level is known as a *transition*, as depicted in Fig. 9.3. Generally, the infrared spectroscopy is principally similar as the other absorption spectroscopy. The lower energy radiation in the infrared (IR) region of the electromagnetic spectrum can interact with atoms, and molecules can produce changes within these entities. This type of radiation is not energetic enough to excite electrons, but it can cause the chemical bonds in molecules to vibrate in different ways. The absorption of IR radiation is also quantized like other absorption process. In a quantized process, the molecule absorbed only selected frequency. The energy changes in the infrared radiation are in the order of 8–40 KJ/mole (1.9–9.5 KCal/mol). The energy in this range covers the stretching and bending vibrations of various bonds in covalent molecules.

During an absorption process, the molecule absorbed only those frequencies of IR radiation which matched with the natural vibrational frequency of the bonds and hence increases the amplitude of vibrational modes of the molecules. However, all the bonds in a molecule cannot absorb the IR radiation irrespective to the matching frequency of IR radiations, until and unless it has a net dipole moment.

9.3.1 Modes of Vibrations

Organic molecules mostly contain covalent bonds between the atoms, which are not stiff but rather behave like springs and always agitating at room temperature. This movement of the bonds in molecule gives various modes of vibration. There are two modes of vibrations: stretching and bending vibration. These two are the simplest vibrations in IR active molecules, for instance, the diatomic linear molecule

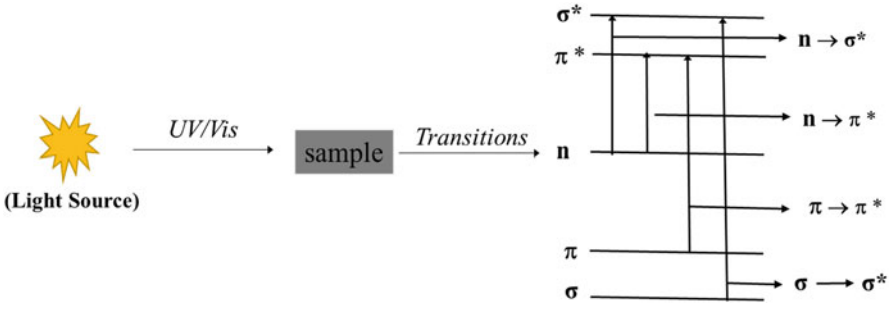

Fig. 9.3 Typical diagram of UV-Vis and electronic transitions under UV-Vis light illuminations

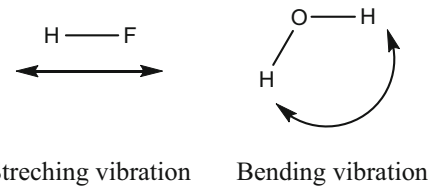

Fig. 9.4 Representation of stretching vibration in diatomic linear molecule hydrogen fluoride (H-F) and bending vibration in triatomic molecule water (H_2O)

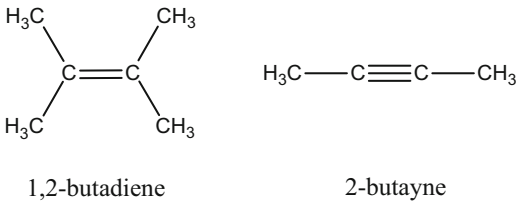

Fig. 9.5 IR inactive molecules with double and triple bond

H-F showing stretching vibration and triatomic H_2O molecule showing bending vibration as depicted in the inset of Fig. 9.4.

However, other complex types of stretching and bending vibration also occurred in IR active molecules. Symmetric and asymmetric vibrations are the types of stretching vibration, while wagging, rocking, twisting, and scissoring are the characteristic types of bending vibrations. It is noteworthy that the stretching vibrations usually occurred at higher energy when compared to the bending vibrations. Similarly, among the stretching vibrations, asymmetric stretching vibrations are aroused at higher energy than the symmetric one. Furthermore, this absorption process is quantized; therefore, stretching and bending vibration take place at specific allowed energy levels. However, some molecules absorbed strongly as compared to others, and some even do not absorb at all. Those which absorb IR radiations are called IR active, and those which not absorb IR radiation are called IR inactive molecules. The absorption and strength of absorption depend on the dipole moment of the molecules. For instance, the amplitude of carbonyl group (C=O) stretching frequency is much intense as compared to alkyne (C≡C), because of the fact that the polarity of (C=O) is higher than (C≡C). Some IR inactive vibrations of the molecules containing double and triple bonds are depicted in Fig. 9.5.

9.3.1.1 Stretching Vibration

If a molecule contain at least two or three identical groups, then symmetric and asymmetric stretching arises, for instance, CH_2, CH_3, CCl_2, anhydride, NO_2, and NH_2 groups. The asymmetric stretching has higher energy than the symmetric stretching. In symmetric stretch, the bond lengths of the participating atoms either increase or decrease simultaneously, while in asymmetric stretch one of the bond length increases, while the other decreases. For instance, the CH_3 symmetric stretch arises at approximately 2872 cm^{-1}, while its counterpart asymmetric stretch occurs

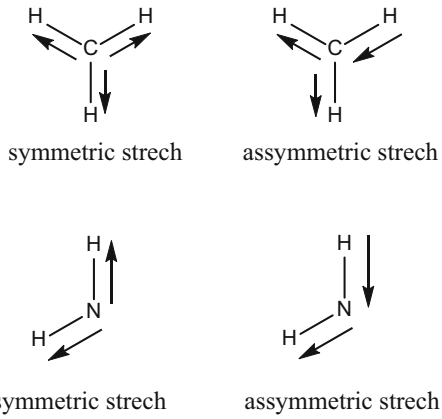

Fig. 9.6 Symmetric stretching and asymmetric stretching vibration of CH_3 and NH_2 groups, where the asymmetric stretch appeared at higher energy

at higher energy (2962 cm^{-1}). Similarly, the symmetric stretch of NH_2 group appears at 3300 cm^{-1} while its asymmetric stretch at 3400 cm^{-1} (Fig. 9.6).

9.3.1.2 Bending Vibration

This type of vibration is also called deformation vibration and causes change in the bond length; however, the bond angle remains the same. There are two types of bending vibrations: (i) in-plane bending and (ii) out-plane bending.

In-plane bending vibration – Scissoring and rocking vibrations are the two types of in-plane bending vibrations. In scissoring vibration both atoms are moving toward each other or away from each other. While in rocking vibration, the bond angles are unchanged due to moments of participating atoms in the same direction, as shown in Fig. 9.7.

Out of plane bending vibration – This vibration includes wagging and twisting vibrations, where the bond angle is changed. In wagging vibration, both the atoms move toward a common side of the plane. While in twisting vibration, both the atoms go opposite to each other. These different types of bending vibrations are presented in Fig. 9.7a, for instance, CH_2 group [15].

9.4 Basic Principle of FTIR

When infrared radiation is bombarded on a sample, it absorbs the light and creates various vibration modes. This absorption relates precisely to the nature of bonds in the molecule. The frequency ranges are measured as wavenumbers typically over the range of 4000–600 cm^{-1}. The FTIR spectrum is measured as wavenumber because wavenumber is directly related to the energy and frequency, thus providing an easy

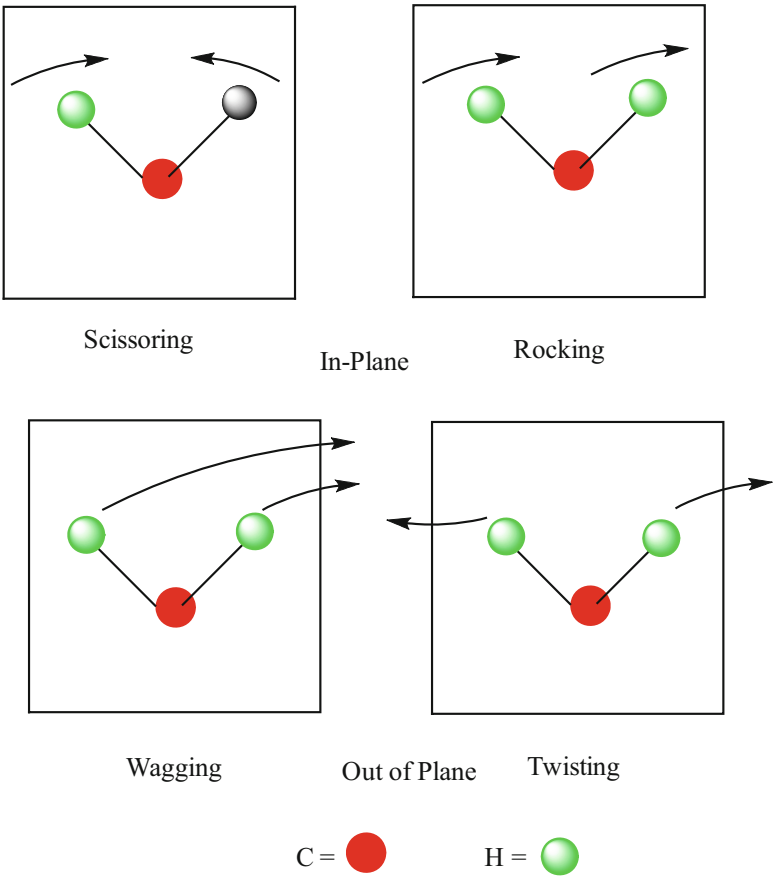

Fig. 9.7 Various modes of bending vibration in methylene group (CH_2). The in-plane comprises the scissoring and rocking vibrations, while the out of plane bending vibrations consist of wagging and twisting

way for interpreting the spectrum. Prior to the sample analysis, the background is recorded, to avoid air and water vapor contamination peaks. The proportion of the background and the sample spectrum are directly related to the absorption spectrum of the sample. The absorption spectrum indicating various vibrations of the bonds presents in the sample molecule. Several modes arise due to the various bond vibrations. So, in this way one can easily identify the functional group in a molecule.

9.5 Instrumentation

The typical FTIR spectrometer consists of an IR light source, interferometer, sample compartment, detector, amplifier, and computer. The light source generates radiation which strikes the sample passing through the interferometer and reaches the detector. Then the signal is amplified and converted to digital signal (interferogram) by the amplifier and analog-to-digital converter, respectively. Eventually, the interferogram is translated to spectrum through the fast Fourier transform algorithm. Michelson interferometer is the main core of FTIR spectrometer and is shown in Fig. 9.8 [12, 16]. The interferometer consists of a beam splitter, fixed mirror, and a moveable mirror that translates back and forth, very precisely. The beam splitter is made of a special material that transmits half of the radiation striking it and reflects the rest half of the radiation. It works on the basis of principle that the light from the source is collected by collimating mirror and made its rays parallel, which strikes beam splitter and consequently splits into two beams. One beam is transmitted through the beam splitter to the fixed mirror, and the second is reflected off the beam splitter to the moving mirror. The fixed and moving mirrors reflect the radiation back to the beam splitter. Accordingly, both of these reflected radiations are recombined at the beam splitter, resulting in one beam that leaves the interferometer and interacts with the sample and strikes the detector, as shown in Fig. 9.8.

Principally, FTIR (Fourier transform infrared) is a method of obtaining infrared spectra, which includes initially the collection of an interferogram of a sample signal using an interferometer and then performance of a Fourier transform (FT) on the

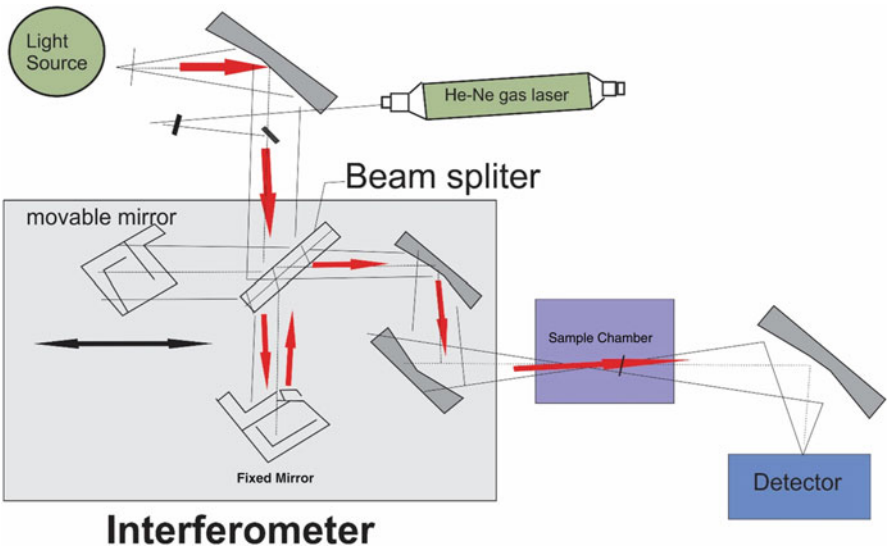

Fig. 9.8 Instrumentation of the double-beam (top) and single-beam (bottom) IR spectrophotometers

interferogram to obtain the spectrum. An FTIR spectrometer collects and digitizes the interferogram, performs the FT function, and displays the spectrum.

9.5.1 Interferometer and Interferogram

The interferometer or interference meter, an optical device, is an important part of the FTIR instrument, which is diagrammatically shown in Fig. 9.8. Principally, the light coming from an infrared source entered the interferometer, where the single light beam splits into two light beams. The interferometer makes these two light beams to travel at different paths, which are denoted by d_1 for beam 1 and d_2 for beam 2, respectively. The optical path difference (OPD) of an interferometer is denoted by the Greek letter small delta (δ), which is the difference in distance traveled by the two light beams. For instance, if the path d_1 is 4 cm long and d_2 is 10 cm long, the optical path difference is 10–4 cm = 6 cm. If the distances of the two light beams travel in the interferometer are identical, then $\delta = 0$, the condition is called zero path difference (ZPD), which occurred when the moving and fixed mirrors are at the same distance from the beam splitter. After traveling of these two beams at their different paths, they recombined into one beam, and then the light beam leaves the interferometer (Fig. 9.8).

The most common type of interferometer used in FTIR nowaday is the Michelson interferometer, named after Albert Abraham Michelson (1852–1931), who first designed this interferometer in the 1880s [17] and win the Nobel Prize in Physics for his discoveries made with it. The Michelson interferometer has already been explained above in the same experimental Sect. 9.5. However, it is important to mention here that how the two light beams recombine into one at the beam splitter. It is usually a characteristic of the waves; they interfere with each other, when they superposed, which means their amplitudes add together to form a single wave. In a Michelson interferometer, the light beams reflected from the fixed and moving mirrors undergo interference, which may be constructive or destructive. If the final amplitude of the resultant beam after interference is greater than the amplitudes of the fixed mirror beam and moving mirror beam, this means that the two beams undergo *constructive interference*. If the final amplitude of the resultant beam is less than the amplitude of either of the two beams, a *destructive interference* has taken place. The square of the amplitude of a light beam is proportional to its intensity. This phenomenon can be explained by a simple example, a candle is usually dim because it gives visible light of low amplitude, and the sun is intense because it gives visible light with high amplitude. When the two light beams in an interferometer interfere with each other (meaning of the word interferometer), the resulting signal pattern obtained called as interferogram.

We are going to explain in a simple understandable way how this interferogram is formed in a Michelson interferometer. It is noteworthy that in case of constructive interference, the optical path difference (OPD) between the fixed mirror and moving mirror beams is $\delta = n\lambda$ ($n = 0, 1. 2$ ..... integral numbers), means that waves

of both beams are in phase with each other and their crests and troughs are overlapped. Therefore, the final amplitude of the resulting interfere wave is greater than the amplitude of either beam wave by itself. Whereas, in case of destructive interference, the OPD between the fixed mirror and moving mirror beams is $\delta = 1/2\lambda$, which means that waves of both beams are out of phase with each other and the crests of the one beam wave are overlapped with troughs of the other one. Therefore, their amplitudes cancel, and the final amplitude is less than the amplitude of either beam wave by itself. Similar phenomenon occurred during the formation of interferogram in the Michelson interferometer.

We simply assume here that a single wavelength light beam passed the interferometer, splits by beam splitter, and undergoes interference to give interferogram. At zero path difference ($\delta = 0\lambda = 0$), the intensity is large because the fixed mirror and moving mirror beams are in phase and constructive interference takes place. As we gradually move ($\delta = 1/2\lambda$) the moving mirror away from the beam splitter, the two beams (fixed and moving beams) grow out of phase with each other, and the resultant beam becomes dimmer due to destructive interference and gives minimum intensity (Fig. 9.9). As the moving mirror continues to move ($\delta = \lambda$), the beams become more in phase, and the resultant beam gains its intensity

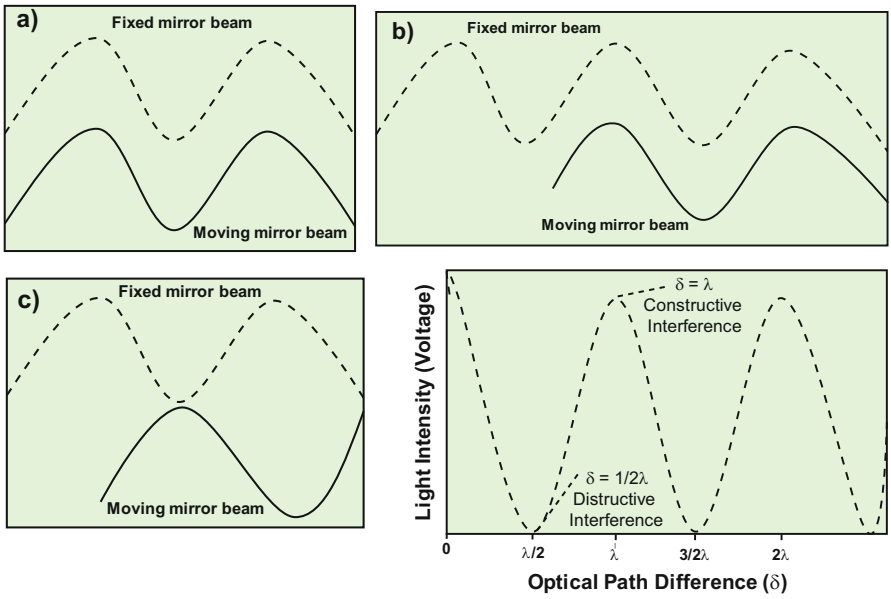

Fig. 9.9 Schematic illustrations of the fixed mirror and moving mirror beams that are present at (**a**) zero optical path distance ($\delta = 0$), in phase and undergoing constructive interference, (**b**) optical path distance of $\delta = \lambda$, undergoing constructive interference, and (**c**) optical path distance of $\delta = 1/2\lambda$, undergoing destructive interference as well as (**d**) interferogram for a single wavelength of light passing through the interferometer, showing a plot of light intensity (or detector signal) versus optical path difference for a mirror moving in a Michelson interferometer [18]

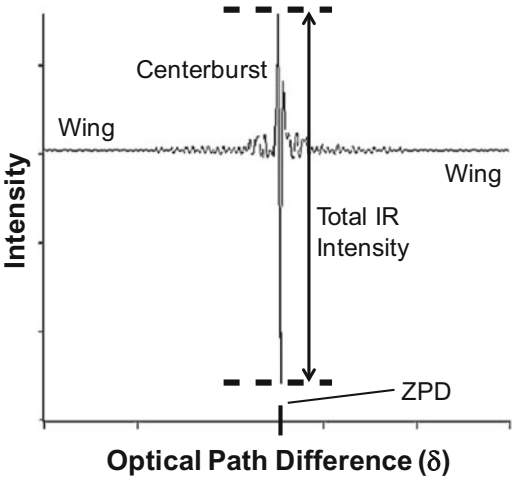

Fig. 9.10 Schematic illustration of the real case interferogram obtained when many wavenumbers of IR light pass through the interferometer together [18]

again. Consequently, the resultant beam intensity grows dimmer and brighter and passes through maxima and minima, as the moving mirror continuously moves. If the measured light intensity versus optical path difference is plotted, the graph obtained is called an *interferogram* (Fig. 9.9), which means "interference writing."

It should be notified that the shape of the interferogram as shown in Fig. 9.10 is a cosine wave and it looks like a light wave, but the interferogram is the electrical signal coming out from the detector. Therefore, the *y*-axis unit in this Figure is presented in voltage. Remember that we have assumed only one wavelength of light passing through the interferometer and making the interferogram. The IR light source through an IR beam containing large number of wavelengths (wavenumbers) passes through the interferometer together. For each of these wavenumbers, there exists an interferogram with a unique Fourier frequency. The detector measures the sum of these individual interferograms, as shown in Fig. 9.10.

It is noteworthy that a large burst of infrared intensity at zero path difference can be observed that is called as *centerburst*. At ZPD all the wavelengths of light are in phase and constructively interfere, consequently giving high-intensity centerburst, which size is proportional to the total amount of infrared light striking the detector. In addition, it can be observed in Fig. 9.10 that as the optical path difference changes, the infrared intensity falls off quickly on both sides of the interferogram called as *wings*. The low intensity of the wings might be due to the increasingly out of phase of the various Fourier frequencies [19] with each other and consequently their destructively interference because of the increasing the optical path difference.

9.5.2 *Fourier Transform of Interferogram to Spectrum*

Fourier transform, named in the honor of French mathematician and physicist Jean Baptiste Joseph Fourier (1768–1830). It is a mathematical method to transform a function into a new function. Fourier transform contains a complicated discussion of mathematics; here we demonstrate to the readers a simple picture that how Fourier transform works qualitatively to convert an interferogram to its spectrum. Please, recall from the above discussion in Sect. 9.5.1 that an interferogram is a superposition of cosine waves. Therefore, when we Fourier transform an interferogram, a new mathematical function is obtained that corresponds to the interferogram. This function is the spectrum of the infrared beam that hits the detector.

It is important to know, when a Fourier transform is applied to a function, the crucial changes that occur are the inversion of the *x*-axis units of that function. For instance, an interferogram is a plot of infrared intensity versus optical path difference (OPD), which can be measured in centimeters as discussed earlier in Sect. 9.5.1. When an interferogram is Fourier transformed, a function is obtained that is a plot of infrared intensity versus cm^{-1}. The unit of wavenumber is cm^{-1}; therefore, a plot of infrared intensity versus wavenumber is an FTIR spectrum as shown in Fig. 9.11. The Fourier transform of any interferogram produces a *single-beam spectrum*, which is a plot of arbitrary infrared intensity versus wavenumber (Fig. 9.11). The term "single beam" is from the fact that there is only one infrared beam used in an FTIR. However, there are some other types of infrared spectrometers, which use two beams.

A single-beam spectrum obtained without a sample is called a background spectrum, which is the characteristic of the instrument and the measuring environment. In this spectrum the characteristic bands around 3500 cm^{-1} and 1630 cm^{-1} are attributed to the atmospheric water vapor, and the bands at 2350 cm^{-1} and 667 cm^{-1} are ascribed to atmospheric carbon dioxide. Therefore, background spectrum must always be run when analyzing sample by FTIR. The single-beam spectrum of the sample obtained after Fourier transformation of interferogram looks similar to the background spectrum except that the peaks of the sample are superimposed upon the instrumental and atmospheric bands. To eliminate these characteristic bands contributed from instrument and atmosphere, the spectrum of the sample must be normalized against the background spectrum. Consequently, a transmittance

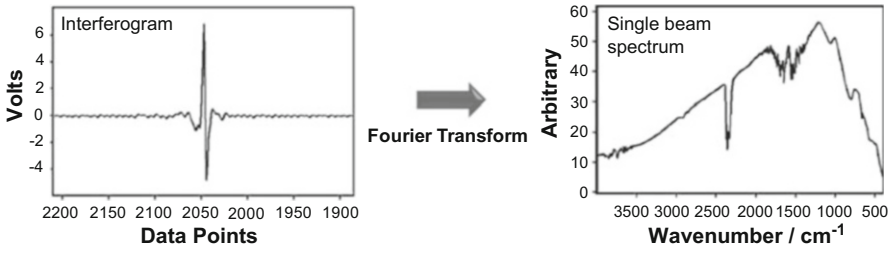

Fig. 9.11 Fourier transform of interferogram to produce a single-beam spectrum [18]

spectrum is obtained as follows:

$$\%T = I/I_0 \tag{9.6}$$

where $\%T$, transmittance; I, intensity of the measured sample in the beam (single-beam spectrum); and I_0, intensity of the background spectrum.

The absorbance spectrum can be calculated from the transmittance spectrum by the following relation:

$$A = -\log_{10} T \tag{9.7}$$

where A is the absorbance.

Therefore, the final transmittance/absorbance spectrum should be devoid of all instrumental and environmental contributions and shows only the characteristic absorption bands of the sample.

9.5.3 Detectors

Detectors convert the thermal or light energy into electrical signal. Thermal and photodetectors are the two main types of detectors used in the FTIR spectrophotometer.

9.5.3.1 Photon Detectors

Semiconductor IR detectors are the most sensitive detectors in the IR spectrometer, which convert photon energy into electrical charge by the internal photoelectric effect. Liquid nitrogen cooled HgCdTe (MCT), InSb, and In(Ga) detectors are a few examples of quantum detectors, which are designed to achieve good performance in FTIR spectrometers. In this class of detectors, the radiation is absorbed within the material which promote the electrons from valence band to the conduction band of the materials resulting in observed electrical output signal. The higher sensitivity is the major advantage of quantum detectors. However, narrower spectral range is the major limitation in quantum detectors. HgCdTe detectors work from 8 to 13 μm of the spectral range. Similarly, PbS and PbSe detectors are sensitive from 1 to 3 μm and 1 to 6 μm, respectively, while the lnSb from 1 to 5.5 μm and lnAs from 1 to 3.5 μm spectral ranges, respectively.

9.5.3.2 Thermal Detectors

This type of detector measures a change in temperature of a material by absorbing the incident electromagnetic radiations. Thermal detectors transformed thermal

energy to electrical signals. Bolometers, thermopiles, thermocouples, pyroelectric, photoacoustic, and pneumatic detectors are some of the most common thermal detectors. Thermal detectors usually used a broad spectral range.

9.5.3.3 Pyroelectric Detectors

Pyroelectric effect is the variation in the spontaneous polarization of a piezoelectric crystal with change in temperature. As compared to the other thermal detectors, the pyroelectric detectors are robust and inexpensive and have comparatively constant sensitivity range through the whole spectral range. Triglycerine sulfate (TGS) and deuterated TGS (DTGS) detectors are common example of pyroelectric detectors. The TGS and DTGS detectors measure the voltage due to the change in temperature by changing their capacitance; however, less sensitivity makes them less efficient.

9.5.3.4 Bolometers

Bolometers detect the change in temperature by changing their resistance. For instance, Si- and Sb-doped Ge semiconductors are the example of bolometer detectors. Bolometers are quite sensitive, but their main disadvantage is the requirement of liquid He as well as their slow process.

Cryogenic bolometers are the most sensitive detectors which can detect from 100 to 1000 μm wavelength range. Such type of detectors converts the light to electric current. Photodiode is the most common high-speed semiconductor detector, which absorbs light and converts it into electrical signals. The signal power limit of the device is resolute by its capacitance and by its junction area. HgCdTe and PbSnTe photodiodes are the examples of high-speed detectors.

9.5.4 Infrared Red Radiation Sources

Different types of lamps are generally used in FTIR with different ranges. For the mid-IR radiation, the silicon carbide is heated to approximately 1200 K. Higher temperature source like tungsten-halogen lamp is used for the near-IR range (shorter wavelengths). The long wavelength output of these is limited to about 5 μm (2000 cm^{-1}) by the absorption of the quartz envelope. For the far-IR, especially at wavelengths beyond 50 μm (200 cm^{-1}), a mercury discharge lamp gives higher output than a thermal source.

9.5.5 Sample Holders in FTIR

There are several types of sample holders used in the FTIR spectrometer as explained below:

Universal sample holder – It is constructed in a spring-loaded mechanism that easily placed KBr pellets, salt plates, films, and other materials. The holder's aperture is 10–20 mm with high sample mounting controllability.

Heavy-duty magnetic film holder – This type of holder is made up of polymer materials. This holder has 20 mm hole with big size steel plate and magnet.

Magnetic film/pellet holder – This type of holder is designed to keep thin polymer films having 0.5 mm size and KBr pellets with 13 mm thickness, comprising of an elastic magnetic strip and steel plate.

Press-on demountable cell holders – It is used for the investigation of mull and smears. 25 mm and 38 mm versions are available and both form containing pressure cap and mounting plate.

Single-pellet holder – This type sample holder is more convenient as compared to dual-pellet holder in virtue of its 7 mm pellets. The PIKE Technologies Hand Press and Pixie Hydraulic Press used this technology.

Dual-pellet holder – Its features are 1, 3, and 7 mm KBr pellet semicircular supports with holes and are helpful in the specified size pellets. The PIKE Technologies Sampling Cards are low-cost sample holders for the examination of polymers, films, and KBr pellets (13 mm). The cards deal with compressed and a suitable means of sample storage.

Bolt press and gas cell holders – These holders are used to mount large sample and salt plate. Three different forms of these holders are available with supported rods having different sized fixtures and are easily separable.

9.5.6 Sample Preparation

The sample preparation is very important for IR spectra analysis where the sample is placed in the cell or in the holder. It is very problematic because IR radiations are strongly absorbed by glass and plastic materials throughout the entire IR range. The cell is constructed of ionic materials, such as KBr or NaCl. The KBr plates are expensive, but they have advantages over NaCl, as they can record IR spectra from 400 to 4000 cm^{-1}. However, NaCl plate is also largely used due to its low cost and recorded spectra from 650 to 4000 cm^{-1}. NaCl is absorbed at 650 cm^{-1}, and very few bands are supposed to absorb in this region; therefore, it is commonly used in the routine experiment. The CO_2 and H_2O from the atmosphere usually appeared in the compound spectrum which causes problem during the interpretation of the spectrum. Therefore, it is very important to run background spectrum so that it is automatically subtracted from the compound spectrum. Between the polished NaCl or KBr plates, a drop of liquid is placed, known as salt plate. After pressing

the plates, a thin film is formed. The pair of plates is inserted in the holders. The spectrum obtained during this method is called as neat spectrum because it is free of solvent. Moreover, being ionic in nature, these salt plates are easily soluble in water; therefore, it is recommended that the compounds must be free of water.

Three methods are available for solid sample. In the first method, the compounds are finely grounded with KBr salt and then pressed at high pressure to form pellets called KBr pellets. However, KBr absorb water which gives water peaks in the spectrum and hindered the peaks originated from the compounds. Nevertheless, if KBr plates are prepared carefully by avoiding the absorption of moisture, no peak will appear in the spectrum. The other advantage is that KBr is transparent below 400 cm^{-1}.

In another method called Nujol mull, the compound is finely grounded with the mineral oil called Nujol, as a result a thick suspension is formed which is placed between the plates. The main drawbacks of this method are the Nujol peaks which appeared at 2924, 1462, and 1377 cm^{-1} that might interfere with for compounds having peak in these regions. In the third method, the compound is dissolved in solvent. Chloroform (CCl_4) is mostly used, because it dissolves most of the organic compounds; however, like Nujol the CCl_4 peaks appeared and interfere with the compounds peak at approximately 700 cm^{-1}.

9.6 IR-ATR (Attenuated Total Reflection)

Due to the drawbacks associated with KBr pellets and liquid cells method, FTIR measurements are largely achieved in attenuated total reflection (ATR) mode because of its simplicity as compared to the conventional transmission mode. Various samples such as liquids, solids, pastes, fiber pellets, powders, slurries, and many other are placed without any treatment on the ATR crystal. It is a fast technique and the data is obtained in a few seconds. This can be achieved practically without any major sample preparation. IR-ATR provided an advantage that the sample can be investigated without interruption. Thus, biofilm removal from its support, which modifies its structure significantly from its natural form, can be avoided. Additionally, very thin films and surface coverings can be examined, which are not available to normal chemical approaches. Particularly ATR is an extremely good technique for polymer and membrane science. The key advantage of ATR is its aptitude for the measurement of varieties of samples such as solid and liquid samples without the need of complex steps.

In this approach, the IR ray enters the ATR crystal at 45° relative to the crystal surface and is entirely reflected at the crystal to sample interface. Because of its wavelike properties, the light is not reflected directly by the boundary surface but by a computer-generated layer within the optically less dense sample. Evanescent wave is a fraction of light which reached to the sample. The penetration depth depends on the wavelength, the refractive indices of the ATR crystal and the sample, as well as the angle of the incident light. Characteristically, it is of the order of a few microns

(0.5–3 μm). The evanescent wave is attenuated in the spectral regions, where the sample absorbs energy. After one or numerous internal reflections, the IR beam exits the ATR crystal and is directed to the IR detector.

9.6.1 Instrumentation of ATR-FTIR

The ATR units are designed as horizontal crystals with a type of fastening usefulness that guarantees good contact between sample and solids. In case of liquid or viscous material, a small drop of the sample is sufficient for its measurement. Crystal constituents are mostly made up of zinc selenide (ZnSe), diamond, and germanium.

For liquid and "soft" samples analysis, ZnSe is appropriate because it is an inexpensive material; however, scratches are made on ZnSe and can only be used between pH 5 and pH 9. For the study of highly absorbing colored samples such as rubbers and carbon black, germanium material is the choice due to its high refractive index. Similarly, for high-surface sensitivity, like thin layers, Ge is perfect because of its low penetration depth. Diamond is chemically inert and also an ideal substance for the manufacturing of crystal surface materials. Although making the crystal material from diamond is quite expensive, however, the reliability of the instrument due to the high resistance of diamond to cut and scrap and its complete insolubility make diamond an ideal material for ATR-FTIR crystal formation. The stepwise procedure for an ATR is as follow: (i) clean the crystal (e.g., with a cellulose tissue and isopropanol); (ii) then measure the instrument background within the ATR unit; and (iii) after that place the sample on the crystal confirming the good contact, record the sample, and save the document.

9.7 FTIR for Materials Characterization

FTIR is an efficient spectroscopic technique to characterize the structure of the following materials.

9.7.1 Organic Compounds

FTIR is largely used for the study of organic molecules, which brought mainly two types of changes in the molecules: stretching vibration causes of change in the bond length and bending vibration causes of change in the bond angle. Change in the bond length usually occurred at higher frequency or energy because stretching required higher energy as compared to bending vibrations. According to Hooke's law, increasing the mass of the atoms will vibrate the atoms at lower frequency or lower energy. For instance, in organic molecules the most common bonds in the

Table 9.2 Range in wavenumber (cm^{-1}) of various functional groups

Range (cm-1)	Functional group
3200–3550	O-H stretching
2500–3000	Carboxylic O-H
3300–3500	N-H stretch, primary amine gives two, secondary one, while tertiary amine gives no peak
3500–3500	O=C-N-H stretch
2260–2220	Nitrile (CN)
2950–2850	C-H stretch
3010–3100	=C-H stretch
1620–1680	C=C stretch
1740–1690	Aldehyde C= O
1750–1680	Ketone C = O
1750–1735	Ester C = O
1780–1710	Carboxylic acid C=O
1690–1630	Amide C=O
2800–2700	Aldehyde C-H stretch

molecule are C-C, C-H, C-X, C-O, C-N, etc. While dealing the FTIR spectrum of compounds containing C-H, C-D, and C-C bonds, the stretching vibration of C-H (2900 cm^{-1}) appeared at higher frequency as compared to C-D (2100 cm^{-1}) and C-C at (1200 cm^{-1}); the same order is true for bending vibrations. If the molecule has C-F, C-Cl, C-Br, and C-I, the stretching vibration will appear as C-F > C-Cl > C-Br > C-I (descending order of energy). The molecule containing multiple different bonds, for instance, C-C, C=C, and C≡C, the absorption will occur according to the strength of bonds, for example, triple bond is more stronger as compared to double and single, so the C≡C stretching vibration will appear at 2200 cm^{-1}, C=C at 1600 cm^{-1}, and C-C bond at 1200 cm^{-1}, respectively.

For the organic molecule, the infrared spectrum can be usually divided into four parts (Table 9.2):

(i) 4000–2500 cm^{-1}: Single bonds absorption of hydrogen with other elements, e.g., O-H, N-H, and C-H.
(ii) 2000–2500 cm^{-1}: Triple bonds absorption, C ≡ C and C ≡ N.
(iii) 1500–2000 cm^{-1}: Double bonds absorption, e.g., C=C and C=O.
(iv) 400–1500 cm^{-1}: The region from 1000 to 1500 cm^{-1} is usually used for C-O and C-C and other bending vibrations. The region 700–400 cm^{-1} is usually called the fingerprint region which is unique for various compounds and rarely used for the identification of functional groups.

The H-X bonds are more prominent in the organic molecules. For instance, the C-H asymmetric stretching vibrations appeared at approximately 2900 cm^{-1}. There are different types of C-H stretching vibration, for instance, in case of unsaturated vibrations, the C-H sp (H-C≡C) will appear at approximately 3300 cm^{-1} due to the higher bond strength of sp bond, while C-H sp^2 (H-C=C) are above 3000 cm^{-1},

and C-H sp^3 are below 3000 cm^{-1}. The different bond strengths and absorptions are explained on the basis of their bond strength, which is due to the increase in s character of these bonds. The aldehyde exhibited two weak bands at 2850 and 2750 cm^{-1}. The C=C of the benzene ring appeared at 1600–1500 cm^{-1}, and the bending vibration of aromatic hydrogen Ar-H appeared at the range of 700 cm^{-1}. Similarly, the CH_3 bending vibrations appeared at 1460 and 1375 cm^{-1}, while the bending vibration of CH_2 appeared at 1465 cm^{-1}. The bending vibrations of CH_3 (asymmetric) and CH_2 are not mostly resolved and overlapped with each other. The O-H vibrations appeared at 3300–3600 cm^{-1}. If the O-H group makes hydrogen bonding to any other group inter- or intramolecular, the bond becomes weak, and a broadband will appear at lower frequency at approximately 3300 cm^{-1}. In case of free O-H (no hydrogen bonding), a sharp peak will appear at approximately 3600 cm^{-1}. The N-H appeared at 3300–3400 cm^{-1}. There are three types of N-H bonds: primary, secondary, and tertiary. The primary N-H gives two peaks, secondary one and tertiary indicating no peak at all.

9.7.2 Nanomaterials

Any solid materials with one of its dimension fewer than about 100 nm are known as nanoscale materials or nanomaterials. Nano is one billionth 10^{-9} and is one millionth of a millimeter. It was revealed that a nanomaterial is almost 100,000 times lesser than the human hair. Nanomaterials size is lying somewhere between the atoms or molecules size and a bulk structure of the molecules [13]. This small size of the particle (one millionth of a millimeter), abruptly, increases the surface/volume ratio, and, therefore, many vital physical and chemical characteristics are expressively improved, which are completely different from their bulk counterparts. Although, nanomaterials and their bulk counterparts organize the same materials, but smaller particles indicate absolutely diverse physicochemical or electromagnetic properties from their bulk counterparts [20]. FTIR spectra of various metal oxide and doped metal oxide are discussed below:

FTIR spectrum of zinc oxide – For ZnO, the absorption peak at 1050 cm^{-1} indicated the presence of Zn-O bond, whereas the peaks at 1406 and 1575 cm^{-1} exhibited the presence of carbonate anion. Moreover, the absorption peak at 3408 cm^{-1} is indicative of O-H stretching vibration. When ZnO is mixed with graphene oxide (GO), some characteristic peak appeared for the GO along with ZnO at 1050, 1621, 1735, and 3436 cm^{-1} due to the C-O bond, carboxyl groups, aromatic structure, and O-H groups, respectively [21]. The general FTIR spectrum for nanomaterials is depicted in the inset of Fig. 9.12.

FTIR spectrum of cobalt oxide – The Co_3O_4 exhibited absorption bands for M-O at 567 cm^{-1}, M-O-M, stretching at 655 cm^{-1}, whereas the absorption peak at 1374 cm^{-1} is indicative of the presence of carbonate ($CO_3{}^{-2}$) anions. If we look at the core-shell structure of Co_3O_4/SiO_2, it displayed various absorption bands at 1605 cm^{-1} for the O-H bond and absorptions from 1086–1320 cm^{-1} due to the presence of SiO_2 [22] as depicted in Fig. 9.12.

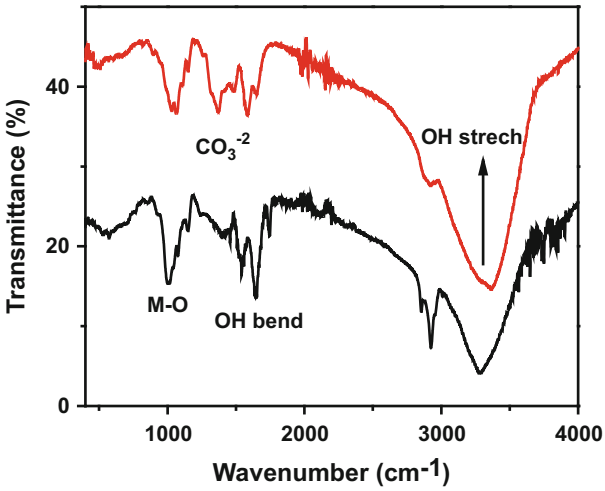

Fig. 9.12 Generalized FTIR spectra of various M-O bond, CO_3^{-2}, and O-H stretching and bending vibration

FTIR spectrum of titanium oxide – The Ti-O bond usually shows absorption band at 818 cm^{-1} in the TiO_2 catalyst, while a sharp band may be observed at 3747 cm^{-1} indicating the O-H group. When TiO_2 is mixed with polyaniline (PANI), some characteristics absorption bands of PANI at 1308, 1494, 1567, 3268, and 3747 cm^{-1} appeared in their FTIR spectrum [23].

FTIR spectrum of iron oxide – The iron oxide displayed absorption peaks at 431 and 525 cm^{-1} which clearly indicated the metal oxide bond in the sample. In the doped Co_3O_4/Fe_2O_3, peaks for M-O appeared along with the presence of carbonate group [22].

FTIR spectrum of cadmium oxide – The CdO absorbance appeared in the FIR spectrum at 462, 542, 780, and 1107 cm^{-1}. A sharp peak at 3435 cm^{-1} in CdO_2 exhibited the stretching vibration of water molecule. The sharp peak indicated the absence of hydrogen bonding, while the bending vibration of H_2O in CdO_2 nanomaterial appeared 1623 cm^{-1} [24] as depicted in Fig. 9.12.

9.8 Applications

9.8.1 FTIR in Biomedical Imaging

FTIR spectroscopic imaging is a chemical imaging technique which is very important to investigate the biological samples. For characterizing the biomedical sample, FTIR spectroscopy has advantages over other imaging techniques because

it detects specific molecular vibrations in the chemical bonds of molecules. FTIR imaging technique does not required the dyes for labeling or visualization in various sample, and its application is largely reported in medical imaging samples [25]. There are several examples which indicate the application of FTIR in medical imaging techniques. For instance, it is used in human colorectal adenocarcinoma studies [26]. Similarly, the deposition of β-amyloid protein in human brain tissue slice, comprises the Alzheimer's diseases, have been investigated through FTIR spectroscopic imaging techniques [27].

The ATR-FTIR imaging technique is important in the biomedical field [28]. Many examples are available in the literature regarding ATR-FTIR in imaging techniques [25, 29]. Thus ATR-FTIR is the key for the potential characterization of biomedical samples in tissue engineering. In the ATR-FTIR mode, the sample preparation is very simple because the penetration depth of IR radiation does not depend on the sample thickness. For reliable and appropriate FTIR images, place the sample directly on the diamond ATR crystal which will result in good interaction of sample with the ATR crystal [30]. The biological tissue such as the aorta, small force is applied to the cross section of the aorta for better images [31]. The FTIR imaging of a brain tumor tissue section is indicated in the inset of Fig. 9.13.

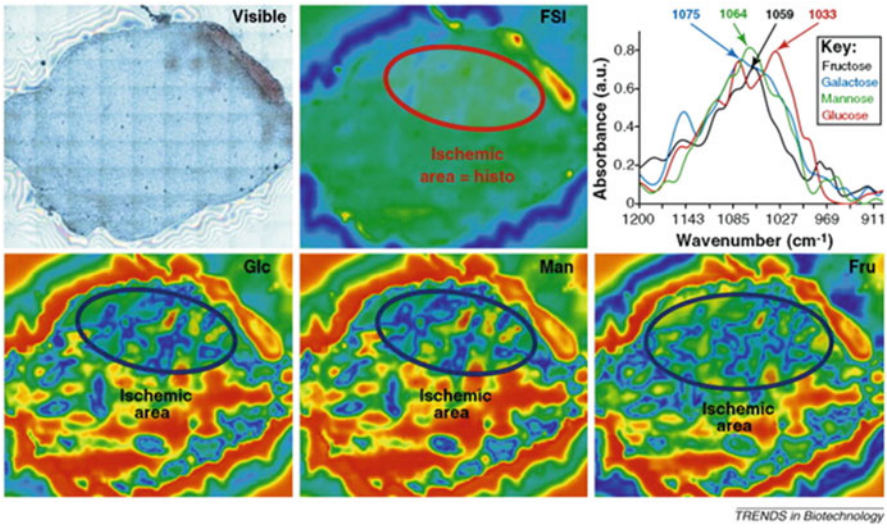

Fig. 9.13 FTIR imaging of a brain tumor tissue section, including full spectral image (FSI; 4000–500 cm^{-1} spectral integration) and chemical mapping of saccharides. The example provided shows that very similar results are obtained on chemical mapping with glucose absorption found at 1033 cm^{-1} (Glc), a mannose absorption band at 1064 cm^{-1} (Man), or a fructose absorption band at 1059 cm^{-1} (Fru) [32]

9.8.2 FTIR in Proteins Study

The infrared spectroscopy came into existence since the discovery of IR radiation in sunlight in 1800 by Sir William Herschel, an astronomer [33]. William Coblentz described the IR spectra of various sample in 1905 [34, 35]. After World War II, advancement occurred in double-beam dispersive IR spectrometer, and thereby IR spectroscopy was considering a common analytical apparatus for the researcher and had been applied in diverse scientific fields, including the characterization of protein molecules [36, 37].

In 1950, the structure of proteins was investigated by Ambrose and Eliot with the use of IR spectroscopy [38, 39]. Similarly, Miyazawa studied N-methylacetamide for the investigation of proteins molecule through IR spectroscopy [40, 41]. The structure of protein was investigated using X-ray crystallography; however, multidimensional NMR spectroscopy can help in the elucidation of protein structure determination. In many cases these techniques cannot be applied properly. In many cases the FTIR can be applied for the structural determination of protein. There are two major bands in the FTIR spectrum of protein known as amide I (1600–1700 cm^{-1}) and amide II. The amide I is the most intense band due to C=O stretching vibration, while amide II is due to the N-H bending vibration and C-N stretching vibration [42].

9.8.3 Miscellaneous Applications of FTIR Spectroscopy

FTIR is an extremely important tool for the detection of large range samples in different fields. For instance, resins, adhesives, paints, coatings, polymers, metal oxides, and large number of drugs can be analyzed with the help of this technique. For instance, different nature samples such as gummy materials, solids, liquids, and solution can be analyzed and identified with the help of FTIR. The identification of diverse range of organic and inorganic compounds can be analyzed through this technique. Polymers and polymer blends as well as indirect verification of trace organic contaminants on surfaces of various materials can be analyzed. Routine qualitative and quantitative analyses can be performed. With the help of FTIR adhesives, coatings and adhesion promoters or coupling agents as well as thin film can be easily analyzed. We can analyze stains and surface blemishes remnant from cleaning and degreasing processes through FTIR in combination with optical microscopy, SEM/EDX, XPS, and SIMS techniques. We can identify rubbers and filled rubbers through this technique, and the degrees of crystallinity in polymers can be determined through FTIR, for instance, low-density polyethene (LDPE) and high-density polyethene (HDPE) can be identified. Similarly, comparative chain lengths in organic molecules can also be differentiated through this method. We can also analyze the gaseous samples using a gas cell for the headspace analysis or environmental monitoring process.

9.9 Conclusion and Future Prospective

The advancement in the FTIR spectroscopy specifically for the characterization of materials is now well-known and is steadily increasing. The capability of FTIR to characterize chemical and biological materials is exponentially arising. In this chapter we provided the in-depth detail about the infrared spectroscopy. Spectral region with respect to infrared, instrumentation, and basic principal of FTIR has been discussed. Sample preparation techniques and various functional group ranges in organic compounds and nanomaterials are explained in detail. Finally, the application of FTIR in various scientific fields has been explored. This chapter will help the readers and scientific community about the detailed and advanced knowledge of infrared spectroscopy. In future prospect we will address the addition of novel accessories to the FTIR and will mechanistically explained the role of FTIR spectroscopy in the biological sample.

Acknowledgment The authors highly acknowledge the Chemistry Department and Center of Excellence for Advanced Materials Research King Abdulaziz University, Jeddah, Saudi Arabia and Department of Chemistry, University of Swabi, Anbar, Khyber Pakhtunkhwa, Pakistan for providing facility.

References

1. Shrivastava, N., Khan, L., Vargas, J., Ospina, C., Coaquira, J., Zoppellaro, G., Brito, H., Javed, Y., Shukla, D., & Felinto, M. (2017). Efficient multicolor tunability of ultrasmall ternary-doped LaF 3 nanoparticles: Energy conversion and magnetic behavior. *Physical Chemistry Chemical Physics, 19*, 18660–18670.
2. Khan, L. U., Brito, H. F., Hölsä, J., Pirota, K. R., Muraca, D., Felinto, M. C., Teotonio, E. E., & Malta, O. L. (2014). Red-green emitting and superparamagnetic nanomarkers containing Fe3O4 functionalized with calixarene and rare earth complexes. *Inorganic Chemistry, 53*, 12902–12910.
3. Herschel, W. (1800). XIII. Investigation of the powers of the prismatic colours to heat and illuminate objects; with remarks, that prove the different refrangibility of radiant heat. To which is added, an inquiry into the method of viewing the sun advantageously, with telescopes of large apertures and high magnifying powers. *Philosophical Transactions of the Royal Society of London, 90*, 255–283.
4. Jacquinot, P. (1954). The luminosity of spectrometers with prisms, gratings, or Fabry-Perot etalons. *JOSA, 44*, 761–765.
5. Fellgett, P. (1958). Equivalent quantum-efficiencies of photographic emulsions. *Monthly Notices of the Royal Astronomical Society, 118*, 224–233.
6. Connes, J. R. (1961). Recherches sur la spectroscopie par transformations de Fourier, Éd. de la" Revue d'optique théorique et instrumentale.
7. Chamberlain, G. (1979). *Analysis of covariance with qualitative data*. Cambridge, MA: National Bureau of Economic Research.
8. Kauppinen, J., & Partanen, J. Frontmatter and index, fourier transforms in spectroscopy, i–ix.
9. Rubens, H., & Wood, R. (1911). XXVII. Focal isolation of long heat-waves. *The London, Edinburgh, and Dublin Philosophical Magazine and Journal of Science, 21*, 249–261.

10. Rubens, H., & Von Baeyer, O. (1911). LXXX. On extremely long waves, emitted by the quartz mercury lamp. *The London, Edinburgh, and Dublin Philosophical Magazine and Journal of Science, 21*, 689–695.
11. Illingworth, K. (1927). A repetition of the Michelson-Morley experiment using Kennedy's refinement. *Physical Review, 30*, 692.
12. Camy-Peyret, C., Flaud, J.-M., Mandin, J.-Y., Chevillard, J.-P., Brault, J., Ramsay, D., Vervloet, M., & Chauville, J. (1985). The high-resolution spectrum of water vapor between 16500 and 25250 cm^{-1}. *Journal of Molecular Spectroscopy, 113*, 208–228.
13. Blakeney, A. B., Harris, P. J., Henry, R. J., & Stone, B. A. (1983). A simple and rapid preparation of alditol acetates for monosaccharide analysis. *Carbohydrate Research, 113*, 291–299.
14. Kauppinen, J. (1979). Working resolution of 0.010 cm^{-1} between 20 cm^{-1} and 1200 cm^{-1} by a Fourier spectrometer. *Applied Optics, 18*, 1788–1796.
15. Chen, Y., Zou, C., Mastalerz, M., Hu, S., Gasaway, C., & Tao, X. (2015). Applications of micro-fourier transform infrared spectroscopy (FTIR) in the geological sciences—a review. *International Journal of Molecular Sciences, 16*, 30223–30250.
16. Genzel, R., Lutz, D., Sturm, E., Egami, E., Kunze, D., Moorwood, A., Rigopoulou, D., Spoon, H., Sternberg, A., & Tacconi-Garman, L. (1998). What powers ultraluminous IRAS galaxies? *The Astrophysical Journal, 498*, 579.
17. Livingston, D. M. (1973). *The master of light: A biography of Albert Abraham Michelson*. Chicago: The University Press of Chicago.
18. Smith, B. C. (2011). *Fundamentals of fourier transform infrared spectroscopy*. Boca Raton: CRC press.
19. Johnston, S. F. (1991). *Fourier transform infrared: A constantly evolving technology*. New York: Ellis Horwood.
20. Ng, L. Y., Mohammad, A. W., Leo, C. P., & Hilal, N. (2013). Polymeric membranes incorporated with metal/metal oxide nanoparticles: A comprehensive review. *Desalination, 308*, 15–33.
21. Yao, H., Li, F., Lutkenhaus, J., Kotaki, M., & Sue, H.-J. (2016). High-performance photocatalyst based on nanosized ZnO-reduced graphene oxide hybrid for removal of rhodamine B under visible light irradiation. *AIMS Materials Science, 3*, 1410.
22. Khan, S. A., Khan, S. B., & Asiri, A. M. (2015). Core–shell cobalt oxide mesoporous silica based efficient electro-catalyst for oxygen evolution. *New Journal of Chemistry, 39*, 5561–5569.
23. Hidalgo, D., Bocchini, S., Fontana, M., Saracco, G., & Hernández, S. (2015). Green and low-cost synthesis of PANI–TiO 2 nanocomposite mesoporous films for photoelectrochemical water splitting. *RSC Advances, 5*, 49429–49438.
24. Thema, F., Beukes, P., Gurib-Fakim, A., & Maaza, M. (2015). Green synthesis of monteponite CdO nanoparticles by Agathosma betulina natural extract. *Journal of Alloys and Compounds, 646*, 1043–1048.
25. Kazarian, S., & Chan, K. (2006). Applications of ATR-FTIR spectroscopic imaging to biomedical samples. *Biochimica et Biophysica Acta (BBA) – Biomembranes, 1758*, 858–867.
26. Lasch, P., Boese, M., Pacifico, A., & Diem, M. (2002). FT-IR spectroscopic investigations of single cells on the subcellular level. *Vibrational Spectroscopy, 28*, 147–157.
27. Choo, L.-P., Wetzel, D. L., Halliday, W. C., Jackson, M., LeVine, S. M., & Mantsch, H. H. (1996). In situ characterization of beta-amyloid in Alzheimer's diseased tissue by synchrotron Fourier transform infrared microspectroscopy. *Biophysical Journal, 71*, 1672–1679.
28. Sommer, A. J., Tisinger, L. G., Marcott, C., & Story, G. M. (2001). Attenuated total internal reflection infrared mapping microspectroscopy using an imaging microscope. *Applied Spectroscopy, 55*, 252–256.
29. Kazarian, S. G., & Chan, K. A. (2006). Sampling approaches in fourier transform infrared imaging applied to polymers, *Characterization of polymer surfaces and thin films* (pp. 1–6). Springer. Berlin, Heidelberg.

30. Chan, K., & Kazarian, S. (2003). New opportunities in micro-and macro-attenuated total reflection infrared spectroscopic imaging: Spatial resolution and sampling versatility. *Applied Spectroscopy, 57*, 381–389.
31. Colley, C., Kazarian, S., Weinberg, P., & Lever, M. (2004). Spectroscopic imaging of arteries and atherosclerotic plaques. *Biopolymers, 74*, 328–335.
32. Petibois, C., & Desbat, B. (2010). Clinical application of FTIR imaging: New reasons for hope. *Trends in Biotechnology, 28*, 495–500.
33. Herschel, W. (1801). Observations tending to investigate the nature of the sun, in order to find the causes or symptoms of its variable emission of light and heat; with remarks on the use that may possibly be drawn from solar observations. *Philosophical Transactions of the Royal Society of London, 91*, 265–318.
34. Coblentz, W. W. (1905). *Investigations of infra-red spectra*. Washington, DC: Carnegie institution of Washington.
35. Smith, A. L. (1979). *Applied infrared spectroscopy: Fundamentals, techniques, and analytical problem-solving*. New York: Wiley.
36. Rothschild, K. J. (2016). The early development and application of FTIR difference spectroscopy to membrane proteins: A personal perspective. *Biomedical Spectroscopy and Imaging, 5*, 231–267.
37. Derrick, M. R., Stulik, D., & Landry, J. M. (2000). *Infrared spectroscopy in conservation science*. Los Angeles: Getty Publications.
38. Elliott, A., & Ambrose, E. (1950). Structure of synthetic polypeptides. *Nature, 165*, 921–922.
39. Elliott, A., Ambrose, E., & Robinson, C. (1950). Chain configurations in natured and denatured insulin: Evidence from infra-red spectra. *Nature, 166*, 194–194.
40. Anderson, D., & Bellamy, L. J. (1975). *The infrared spectra of complex molecules*. London: Chapman and Hall xix+ 433 pp., price£ 8.00, Elsevier, 1976.
41. Miyazawa, T., & Shimanouchi, T. (1958). S.i. Mizushima, normal vibrations of N-methylacetamide. *The Journal of Chemical Physics, 29*, 611–616.
42. Jabs, A. (2005). Determination of secondary structure in proteins by fourier transform infrared spectroscopy (FTIR), Jena Library of Biological Molecules [online][cited 16. 2. 2011]. Available online: http://www.imbjena.de/ImgLibDoc/ftir/IMAGE_FTIR.html.